https://doi.org/10.5194/hess-2021-181
Preprint. Discussion started: 18 May 2021

Hydrology and Earth System Sciences
Open Access
EGU
Discussions

Sequential Data Assimilation for Real-Time Probabilistic Flood Inundation Mapping

Keighobad Jafarzadegan*, Peyman Abbaszadeh, Hamid Moradkhani

Center for Complex Hydrosystems Research, Department of Civil, Construction, and Environmental Engineering, University of Alabama, Tuscaloosa, AL

*Corresponding author: kjafarzadegan@ua.edu

https://doi.org/10.5194/hess-2021-181
Preprint. Discussion started: 18 May 2021

Hydrology and Earth System Sciences
Discussions

Abstract

Real-time probabilistic flood inundation mapping is crucial for flood risk warning and decision making during the emergency of an upcoming flood event. Considering high uncertainties involved in the modeling of a nonlinear and complex flood event, providing a deterministic flood inundation map can be erroneous and misleading for reliable and timely decision making. The conventional flood hazard maps provided for different return periods cannot also represent the actual dynamics of flooding rivers. Therefore, a real-time modeling framework that forecasts the inundation areas before the onset of an upcoming flood is of paramount importance. Sequential Data Assimilation (DA) techniques are well-known for real-time operation of physical models while accounting for existing uncertainties. In this study, we present a ~~Data Assimilation (~~DA~~)~~-hydrodynamic modeling framework where multiple gauge observations are integrated into the LISFLOOD-FP model to improve its performance. This study utilizes the Ensemble Kalman Filter (EnKF) in a multivariate fashion for dual estimation of model state variables and parameters where the correlations among point source observations are taken into account. First, a synthetic experiment is designed to assess the performance of the proposed approach, then the method is used to simulate the Hurricane Harvey flood in 2017. Our results indicate that the multivariate assimilation of point-source observations into hydrodynamic models can improve the accuracy and reliability of probabilistic flood inundation mapping by 5-7% while it also provides the basis for sequential updating and real-time flood inundation mapping.

Keywords: Data Assimilation; Probabilistic Flood Inundation Mapping; Hydrodynamic Model; Ensemble Kalman Filter

https://doi.org/10.5194/hess-2021-181
Preprint. Discussion started: 18 May 2021

Hydrology and Earth System Sciences
Open Access
Discussions

1. Introduction

The on-time, accurate, and reliable characterization of an upcoming flood event is imperative for proper decision making and risk analysis. A well-calibrated hydrologic model coupled with reliable weather forecast models can be used to generate the streamflow forecast (Clark and Hay, 2004; Cuo et al., 2011; Habets et al., 2004). While streamflow forecasting during flood events is indispensable, the critical step for flood risk analysis is to estimate the flood inundation areas corresponding to the forecasted streamflow of a potential upcoming event. Hydrodynamic models are common tools used to simulate the physics of a river system and predict the spatiotemporal distribution of water surface elevation. The predicted water surface elevation can be simply converted to water depth and inundation area by overlaying with a high-resolution Digital Elevation Model (DEM) (Merwade et al., 2008; Teng et al., 2017).

According to the literature, most studies have analyzed the flood events for which the flood extent maps were available from surveying or satellite remote sensing. These studies include but are not limited to, calibration and assimilation of hydrodynamic models (Baldassarre et al., 2009; García-Pintado et al., 2013; Gobeyn et al., 2017; Hostache et al., 2009; Lai et al., 2014; Pappenberger et al., 2007; Rahman and Thakur, 2018; Tarpanelli et al., 2013). Depending on the ~~research~~ objectives, such studies are crucial as they address important theoretical questions and advance the flood modeling task. For example, several studies have used satellite remote sensing data, such as Synthetic Aperture Radar (SAR) images, to find the sensitivity of hydrodynamic models to their parameters, compare calibration strategies and test the application of assimilating remote sensing data into these models (Di Baldassarre et al., 2009; Hunter et al., 2005; Mason et al., 2009; Matgen et al., 2010). Since floods happen in a short period and at a certain location, it is ~~most~~ often not possible to find an appropriate remote sensing image that covers those inundated areas during the flood period. This is the main reason that research on flood inundation mapping is mostly limited to post-event analysis where specific study areas with available remote sensing data are used as testbeds.

Federal Emergency Management Agency (FEMA) is the leading agency in the United States that provides flood hazard and risk maps over the Contiguous United States (CONUS). These maps display the flood-prone areas corresponding to specific return periods (e.g. 100 and 500-year events). While the FEMA flood hazard and risk maps provide general information about risk areas, they are not always reliable for an upcoming flood event with different return periods. For example, FEMA 100-year and 500-year flood hazard maps covered only one-third and half of the inundated areas induced by Hurricane Harvey in Harris County, Texas, respectively (Pinter et al., 2017). The National Water Center Innovators Program proposed the idea of real-time flood inundation mapping across the United States in 2015 (Maidment, 2017). It highlighted the importance of event-based flood inundation mapping where a model uses the forecasted river discharge to estimate the inundation areas corresponding to a specific flood just before the onset of the event. Compared to the traditional flood hazard mapping, real-time flood inundation mapping is more informative and beneficial for emergency response-related decision-making.

In real-time flood inundation mapping, the model takes advantage of forecasted forcing data and generates inundation areas corresponding to an upcoming flood event. Providing these maps ahead of time is extremely valuable for building a robust flood warning system. Data assimilation (DA) is an effective approach commonly used to improve the performance of real-time hydrologic forecasting by updating the model state variables and parameters when new observation becomes available (Moradkhani et al., 2019). The integration of DA with physical models is highly advantageous as it enables accounting for different sources of uncertainties involved in model

https://doi.org/10.5194/hess-2021-181
Preprint. Discussion started: 18 May 2021

Hydrology and Earth System Sciences
Open Access
EGU
Discussions

predictions. These include (1) forcing data uncertainty due to the limitation of measurements and spatiotemporal representativeness of the data (Alemohammad et al., 2015; Kumar et al., 2017), (2) parameter uncertainty due to equifinality and non-uniqueness of parameters (Abbaszadeh et al., 2018; Leach et al., 2018), (3) model structural uncertainty due to the imperfect representation and conceptualization of a real system (Abbaszadeh et al., 2019; Pathiraja et al., 2018; Zhang et al., 2019) and (4) initial and boundary condition uncertainty (DeChant and Moradkhani, 2014; Lee et al., 2011).

Probabilistic forecasting and uncertainty quantification using DA have been the core of modeling in the atmospheric and oceanic sciences (e.g. Anderson and Anderson, 1999; Courtier et al., 1993). Later, the hydrologic community started to utilize this approach to account for the uncertainties involved in different layers of model predictions and provide more accurate and reliable model estimates such as soil moisture (Pauwels et al., 2001; Reichle et al., 2002), streamflow (Moradkhani et al., 2005a; Vrugt et al., 2006), snow (Sheffield et al., 2003; Slater and Clark, 2006) and so many other variables. Despite these advances in hydrologic studies, the application of data assimilation in conjunction with hydrodynamic models has received little attention in the literature. The characterization of uncertainty in hydrodynamic models for probabilistic flood inundation mapping has been mostly limited to conventional techniques, such as ~~random~~ Monte Carlo sampling (Domeneghetti et al., 2013; Neal et al., 2013; Pedrozo-Acuña et al., 2015; Purvis et al., 2008) and Generalized Likelihood Uncertainty Estimation (GLUE) (Aronica et al., 2002a; Romanowicz and Beven, 2003).

The effectiveness and application of assimilating remotely sensed data (e.g. Soil Moisture Active Passive (SMAP)) into hydrologic models have been vastly investigated in the literature (Abbaszadeh et al., 2020; Azimi et al., 2020; Lievens et al., 2017). However, given the small scale

https://doi.org/10.5194/hess-2021-181
Preprint. Discussion started: 18 May 2021

of the hydrodynamic modeling process, the spatiotemporal resolution of current satellite products is not adequate for assimilating into these models. To properly estimate the flood inundation extent, a spatial resolution less than river width (e.g. 100 m) is recommended. In addition, due to the short duration of floods, satellite data with daily revisit time is needed. Since remote sensing products do not provide such high spatiotemporal resolution data for hydrodynamic models, the research on hydrodynamic data assimilation is limited in the literature. Due to the coarse spatial resolution of satellites that provide water surface elevation data, some studies have limited their analyses to large rivers with a width of above 1 km (e.g. study of Nile and Amazon) (Brêda et al., 2019). However, since the width of the majority of rivers is less than 100 meters, these studies cannot be practically used in many regions. Several studies used higher resolution synthetic SWOT data to evaluate the performance of assimilation techniques (Durand et al., 2008; Munier et al., 2015; Pedinotti et al., 2014; Yoon et al., 2012). While these works provided important information about the assimilation of satellite data into hydrodynamic models, their applications are only limited to synthetic experiments, making them impractical for real case studies. Some studies have implemented indirect methods to estimate WSE from flood extents generated by high-resolution SAR satellite data (Giustarini et al., 2011; Hostache et al., 2010; Matgen et al., 2010b; Neal et al., 2009). This approach can provide high-resolution data that is suitable for the majority of rivers. However, the reliability of this data is concerning because the methods used to convert the flood extent to WSE pose additional errors ~~which~~ downgrades the quality of the final observed data for assimilation practices. Besides these issues, the major drawback of remote sensing data assimilation pertains to their coarse temporal resolutions. To efficiently monitor the flood dynamics, the assimilation process should be performed at a daily/hourly time scale, however, the revisit frequency of satellites used for capturing the ~~water surface elevation~~ ranges from a week to

https://doi.org/10.5194/hess-2021-181
Preprint. Discussion started: 18 May 2021

a month. Therefore, there is a significantly low chance to capture multiple real-time remote sensing images for the majority of inundated catchments during flood events. In the most optimistic scenario, assimilation of satellite data is only limited to one/two updates during the simulation period ~~which~~ may not be sufficient for reliable probabilistic flood inundation mapping.

Application of DA in hydrodynamic modeling can be either river monitoring or flood inundation mapping. The goal of hydrodynamic data assimilation for river monitoring is to track variations in the channel roughness and bathymetry in the long run. Therefore, the weekly/monthly satellite data can be well assimilated into the models as the channel characteristics do not change on a daily basis. On the other hand, flood inundation mapping needs an hourly/daily track of WSE because floods happen rapidly and affect the river dynamics on a short time-scale. The literature indicates those studies that assimilated data into hydrodynamic models have been mostly designed for river monitoring (Brêda et al., 2019; Durand et al., 2008; Yoon et al., 2012b). To capture the daily dynamics of ~~the~~ rivers for real-time flood inundation mapping, the discharge and water stage values measured at the gauge stations can be assimilated into the hydrodynamic models. Xu et al., (2017) performed a Particle Filtering (PF) approach to assimilate the water stage data from six gauges into a hydrodynamic model. ~~In order~~ to calculate the particle weights in the filtering process, they assumed that gauge observations are independent. In this study, however, we consider interconnections among the gauge stations and apply multivariate Ensemble Kalman Filter (EnKF) to a 2D hydrodynamic model for better characterization and quantification of uncertainty and further improving the accuracy of model simulations.

Advancing the probabilistic hydrodynamic modeling with DA techniques is a necessary step to fill the gap between hydrology and hydrodynamics. To address this problem, this study aims to explore the capability of a standard sequential DA technique, namely the EnKF, for real-time

https://doi.org/10.5194/hess-2021-181
Preprint. Discussion started: 18 May 2021

Hydrology and Earth System Sciences
Open Access
Discussions

probabilistic flood inundation mapping. ~~The~~ past studies that used DA in conjunction with hydrodynamic models have mostly focused on the quantification of uncertainty in one or two hydrodynamic variables~~ (~~e.g. Giustarini et al., (2011) and Hostache et al., (2018) only investigated the uncertainty in the upstream flow and rainfall respectively; Yoon et al., (2012) focused on the uncertainty of river bathymetry while ignoring the roughness parameter uncertainty~~)~~. In addition, the main application of DA-hydrodynamic modeling framework has been in river monitoring at long-term or water stage forecasting during the flood events (Brêda et al., 2019; Matgen et al., 2010; Xu et al., 2017). However, this study takes one step further and proposes a DA-hydrodynamic modeling framework for real-time probabilistic flood inundation mapping while accounting for all sources of uncertainties involved in the model simulations~~. These include~~ hydrodynamic model parameters (channel roughness and river bathymetry)~~ uncertainty~~, forcing data (river boundary conditions)~~ uncertainty~~, and state variable (water depth)~~ uncertainty~~. Additionally, unlike past works that assimilated either discharge or water stage into the hydrodynamic model, this study performs a multivariate DA to incorporate the observed values of both variables into the hydrodynamic model for a reliable simulation of ~~flooding and its corresponding~~ inundation area.

2 Data and Study area

In this study, we simulate the Hurricane Harvey flood, one of the worst natural disasters in the history of the United States that caused more than 120 billion ~~in~~ ~~damage~~ (https://www.nhc.noaa.gov/data/tcr/AL092017_Harvey.pdf). The Harvey storm hit Texas on August 25, 2017, caused massive precipitation for six continuous days and resulted in extreme flooding condition in Houston and surrounding areas. Given the considerable uncertainties in hydrologic and hydrodynamic processes of such an extreme flood, a deterministic modeling approach with fixed inputs provides erroneous simulations that are highly different from observations. To account for the uncertainties involved in different layers of flood simulation, this study implements a DA-hydrodynamic modeling framework and provides probabilistic flood inundation maps.

Figure 1.a shows the study area that consists of four main channels (blue lines) and eight tributaries (red lines). The upstream and downstream boundary conditions (purple points) are provided from daily streamflow in four USGS gauges ((#08068090, # 08068500, #08068740, #08068780) and water stage time series at the downstream gauge (#08069500). The daily streamflow discharge in two internal gauges (green points #08068800 and #08069000) and water stage time series in the second internal gauge are the observations that ~~will be~~ assimilated into the LISFLOOD-FP model. Figures 1.b and 1.c present the geographic location of the study area~~ within the state of Texas and San Jacinto watershed, respectively~~. To set up the LISFLOOD-FP model, we use a DEM with 120 m spatial resolution. Such a coarse resolution DEM alleviates the computational intensity of the proposed probabilistic hydrodynamic modeling framework. It should be noted that the subgrid solver used for simulation of flood has the advantage of accepting narrow rivers with a width of less than 120 m while the cell sizes are 120 m. In this study, the DA-hydrodynamic modeling framework is parallelized and performed on the University of Alabama High-Performance Computing ~~(UAHPC)~~ cluster.

https://doi.org/10.5194/hess-2021-181
Preprint. Discussion started: 18 May 2021

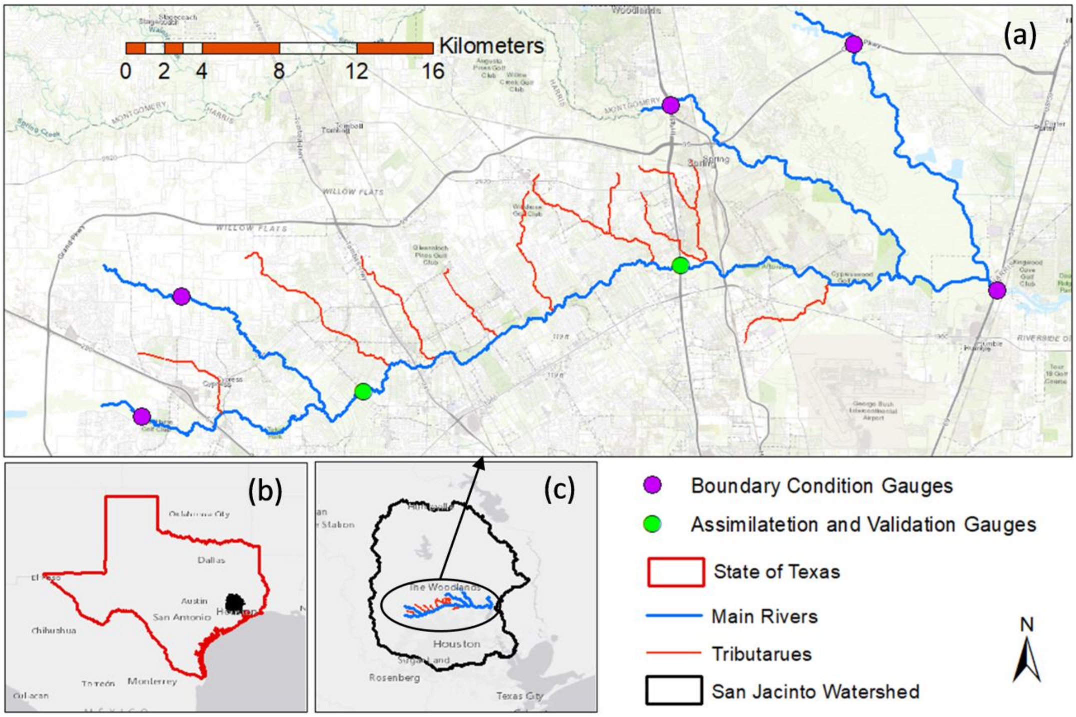

Figure 1 (a) Study area with all gauges, rivers, and tributaries. (b) Geographic location of San Jacinto Watershed within the state of Texas. (c) Geographic location of the study area within San Jacinto watershed (© NhDplus and USGS).

3. Methods

3.1 Flood inundation model

The flood inundation model used in this study is LISFLOOD-FP (Bates and De Roo, 2000), a raster-based 2D hydrodynamic model that simulates the spatiotemporal distribution of ~~water surface elevation~~ over the study area. The model solves the momentum and continuity equations (Saint Venont equations):

$$\frac{\partial Q}{\partial x} + \frac{\partial A}{\partial t} = 0 \quad (1)$$

https://doi.org/10.5194/hess-2021-181
Preprint. Discussion started: 18 May 2021

Hydrology and Earth System Sciences
Discussions

$$\frac{1}{A}\frac{\partial A}{\partial t}+\frac{1}{A}\frac{\partial\left(\frac{Q^2}{A}\right)}{\partial x}+g\frac{\partial h}{\partial x}-g\left(S_0-S_f\right)=0 \qquad (2)$$

where Q is the flow rate at a given cross-section with the area of A in the main channel, x denotes the location along the channel, t represents time, S_0 and S_f are channel bed and friction slopes, and g is the gravitational acceleration.

We use the sub-gird channel solver, the most recently developed numerical scheme that considers friction and water slope as well as local acceleration components in the shallow water equations (Neal et al., 2012). This solver is advantageous for large-scale and efficient modeling as it utilizes coarse resolution DEMs along with channel ~~width values~~ that are smaller than DEM resolution. Since DA-hydrodynamic modeling requires hundreds of model simulations, a computationally intensive operation, this solver helps reduce the computational burden and enables implementing probabilistic flood inundation mapping within a DA framework. To set up the model, we assume rectangular cross-section areas and a uniform roughness for both channel and floodplain. Given the low sensitivity of LISFLOOD-FP to the floodplain roughness (Hall et al., 2005), this parameter is assumed a constant value. However, the channel roughness is the only model roughness parameter whose associated uncertainty is accounted for within the assimilation framework. We also consider the uncertainty of bathymetry by defining an offset parameter that uniformly lowers the DEM values of the river channels. In addition to model parameters (channel roughness and bathymetry), the upstream and lateral fluxes entered the river system as ~~the~~ boundary conditions of the model are other main sources of uncertainty in the assimilation framework.

The upstream boundary conditions are generated from four USGS gauge stations (Figure. 1). To estimate the lateral fluxes, we calculate the deficit in the system as subtraction of the upstream from downstream flows and then, distribute the deficit among river tributaries based on their

https://doi.org/10.5194/hess-2021-181
Preprint. Discussion started: 18 May 2021

Hydrology and Earth System Sciences
Open Access
Discussions

drainage areas (~~Please~~ refer to Jafarzadegan et. al (2021) for detailed information about the calculation of lateral flows in this study area). In section 3.3, we ~~will~~ further discuss the procedure we used to initialize the model parameters and river boundary conditions.

3.2 Ensemble Kalman Filter (EnKF)

~~(~~Moradkhani et al.~~,~~ 2005b) provided a comprehensive description of the EnKF formulation for dual estimation of state and parameters in hydrologic models. Here we briefly describe the EnKF formulation for multivariate assimilation of point source water stage and discharge data into a hydrodynamic model. For a more effective assimilation proccess, both types of interconnections between observations, namely spatial correlation of a single observation (discharge or water stage) among different gauges ~~as well as~~ the correlation between both observations at a single gauge are taken into account in the EnKF equations. ~~In this study,~~ EnKF is used to simultaneously estimate model states and parameters. For this purpose, the parameters should be treated similar to the state variables with a difference that parameter evolution is generated artificially.

~~Let's~~ assume a DA-hydrodynamic modeling framework with l parameters ($p = 1,2,\ldots,l$), m states ($s = 1,2,\ldots,m$) and n observations ($j = 1,2,\ldots,n$). The following EnKF equations are described in accordance with the flowchart shown in Figure 2. In the EnKF, parameter samples can be generated by adding the noise of η_t with covariance $\sum_t^{\theta}$ to the prescribed parameters.

$$\theta_{t+1}^{i-} = \theta_t^{i+} + \tau_t^i \qquad \tau_t^i \sim N(0,\eta_{t+1}) \quad \forall \quad \eta_{t+1} = \textstyle\sum_{t+1}^{\theta} \tag{3}$$

Using θ_{t+1}^{i-} and forcing data, a model state ensemble and predictions are generated, respectively.

$$x_{t+1}^{i-} = f\left(x_t^{i+}, u_t^i, \theta_{t+1}^{i-}\right) + \omega_t^i \quad \omega_t^i \sim N(0,Q_t) \quad \forall \quad Q_t = \textstyle\sum_t^{x} \tag{4}$$

$$\hat{y}_{t+1}^i = h\left(x_{t+1}^{i-}, \theta_{t+1}^{i-}\right) + v_{t+1}^i \qquad v_{t+1}^i \sim N(0,R_{t+1}) \quad \forall \quad R_{t+1} = \textstyle\sum_{t+1}^{y} \tag{5}$$

Hydrology and Earth System Sciences
Open Access
Discussions

where x_t, u_t, θ_t and y_t are the vector of the uncertain state variables, forcing data, model parameters and observation data at time step t, respectively. ω_t represents the model errors due to the imperfect model, and ν_t is the measurement error. Most often, ω_t and ν_t are assumed to be white noises with mean zero and covariance Q_t and R_t, respectively. In addition, the two noises ω_t and ν_t are assumed to be independent.

Then we update the parameter ensemble members using the standard Kalman filter equation:

$$\theta_{t+1}^{i+} = \theta_{t+1}^{i-} + K_{t+1}^{\theta}\left(y_{t+1}^{i} - \hat{y}_{t+1}^{i}\right) \tag{6}$$

where $K_{t+1}^{\theta} \in \mathbb{R}^{l\times n}$ is the Kalman gain matrix for correcting the parameter trajectories and is obtained by:

$$K_{t+1}^{\theta} = \Sigma_{t+1}^{\theta y}\left[\Sigma_{t+1}^{yy} + R'_{t+1}\right]^{-1} \tag{7}$$

where $\Sigma_{t+1}^{\theta y} \in \mathbb{R}^{l\times n}$ is the cross-covariance matrix of parameter ensemble and prediction ensemble (Eq. 6). Unlike other studies, and for more realistic characterization of observation and model errors here the correlation between the errors associated with n observation data are accounted for during the assimilation process. Therefore, the covariance matrix $R'_t \in \mathbb{R}^{n\times n}$ is a nonzero matrix, such that the values in the diagonal represent the error associated with each observation data and all elements lower/upper the main diagonal denote the cross covariance between different observations (Eq. 7). $\Sigma_t^{yy} \in \mathbb{R}^{n\times n}$ is also a similar covariance matrix with the inclusion of error correlation between the model simulations (Eq. 8).

$$\Sigma_{t+1}^{\theta y}(p,j) = \frac{1}{N}\sum_{i=1}^{N}\left[\left(\theta_{t+1}^{i-}(p) - E[\theta_{t+1}^{-}(p)]\right)\left(\hat{y}_{t+1}^{i}(j) - E[\hat{y}_{t+1}(j)]\right)\right] \tag{8}$$

$$R'_{t+1}(j,j') = \begin{cases} R_{t+1} & j = j' \\ \frac{1}{N}\sum_{i=1}^{N}\left[\left(y_{t+1}^{i}(j) - E[y_{t+1}(j)]\right)\left(y_{t+1}^{i}(j') - E[y_{t+1}(j')]\right)\right] & j \neq j' \end{cases} \tag{9}$$

https://doi.org/10.5194/hess-2021-181
Preprint. Discussion started: 18 May 2021

Hydrology and Earth System Sciences
Open Access
EGU
Discussions

$$\Sigma^{yy}_{t+1}(j,j') = \frac{1}{N}\sum_{i=1}^{N}\left[\left(\hat{y}^{i}_{t+1}(j) - E[\hat{y}_{t+1}(j)]\right)\left(\hat{y}^{i}_{t+1}(j') - E[\hat{y}_{t+1}(j')]\right)\right] \tag{10}$$

$$E[\theta^{-}_{t+1}] = \frac{1}{N}\sum_{i=1}^{N}\theta^{i-}_{t+1} \tag{11}$$

$$E[\hat{y}_{t+1}] = \frac{1}{N}\sum_{i=1}^{N}\hat{y}^{i}_{t+1} \tag{12}$$

Now using the updated parameter, the new model state trajectories (state forecasts) and prediction trajectories are generated:

$$x^{i-}_{t+1} = f\left(x^{i+}_{t}, u^{i}_{t}, \theta^{i+}_{t+1}\right) + \omega^{i}_{t} \quad \omega^{i}_{t} \sim N(0, \Sigma^{x}_{t}) \quad \forall \quad Q_t = \Sigma^{x}_{t+1} \tag{13}$$

$$\hat{y}^{i}_{t+1} = h\left(x^{i-}_{t+1}, \theta^{i+}_{t+1}\right) + v^{i}_{t+1} \qquad v^{i}_{t+1} \sim N\left(0, \Sigma^{y}_{t+1}\right) \quad \forall \quad R_{t+1} = \Sigma^{y}_{t+1} \tag{14}$$

Model states ensemble is similarly updated as follows:

$$x^{i+}_{t+1} = x^{i-}_{t+1} + K^{x}_{t+1}\left(y^{i}_{t+1} - \hat{y}^{i}_{t+1}\right) \tag{15}$$

$$y^{i}_{t+1} = y^{i}_{t+1} + v^{i}_{t+1} \qquad v^{i}_{t+1} \sim N(0, R_{t+1}) \quad \forall \quad R_{t+1} = \Sigma^{y}_{t+1} \tag{16}$$

where $K^{x}_{t+1} \in \mathbb{R}^{m\times n}$ is the Kalman gain for correcting the state trajectories and is obtained by:

$$K^{x}_{t+1} = \Sigma^{xy}_{t+1}\left[\Sigma^{yy}_{t+1} + R'_{t+1}\right]^{-1} \tag{17}$$

where $\Sigma^{xy}_{t+1} \in \mathbb{R}^{m\times n}$ is the cross-covariance matrix of states ensemble and prediction ensemble (Eq. 16).

$$\Sigma^{xy}_{t+1}(s,j) = \frac{1}{N}\sum_{i=1}^{N}\left[\left(x^{i-}_{t+1}(s) - E[x^{-}_{t+1}(s)]\right)\left(\hat{y}^{i}_{t+1}(j) - E[\hat{y}_{t+1}(j)]\right)\right] \tag{18}$$

$$E[x^{-}_{t+1}] = \frac{1}{N}\sum_{i=1}^{N}x^{i-}_{t+1} \tag{19}$$

In this study the water depth along the channel is the only state variable (m=1). The channel roughness and bathymetry are two model parameters (l=2) and three point source observations

https://doi.org/10.5194/hess-2021-181
Preprint. Discussion started: 18 May 2021

Hydrology and Earth System Sciences
Discussions

including water discharge at gauge 1 and 2 as well as water stage at gauge 2 (n=3) are assimilated into the LISFLOOD-FP model (Table 1). Therefore, the Kalman gains used to update the model parameters and states (Eqs 5 and 15) are 2×3 and 1×3 matrices that take advantage of a multivariate point source assimilation while considering the downstream correlation between discharge observations and the correlation between water stage and discharge at gauge 2.

3.3. Experimental design

~~The ultimate goal of this study is to simulate the Hurricane Harvey flood and generate probabilistic flood inundation maps through the DA-hydrodynamic modeling framework.~~ Figure. 1 illustrates the flowchart of the proposed probabilistic flood inundation mapping approach. ~~In this study,~~ the EnKF is performed based on an ensemble size of 100. The boundary conditions including four upstream flows, seven lateral fluxes, and downstream flows are perturbed with adding white noises sampled from a normal distribution with a mean zero and relative error of 20%. The errors are assumed heteroscedastic meaning that their values are proportional to the flow magnitude. To characterize uncertainty in the initial condition, namely water depth, we add a white noise with a mean zero and standard deviation of 1 meter. In this study, using the proposed EnKF-based multivariate assimilation approach, three point-scale observations, i.e., discharge at USGS gauges 1 and 2, as well as water stage at gauge 2, are incorporated into the LISFLOOD-FP model to rectify its state variables and parameters, and hence provide more accurate and reliable flood inundation maps. All these three observations are perturbed by adding a normally distributed white noise with a mean zero and a relative error of 20%. First, the LISFLOOD-FP model is forced with the upstream, downstream and lateral flow ensembles. To initialize the state variables in the system, the simulated water depth values at the ending day of the warm-up period (the initial condition for the first day of the model simulation) are perturbed with adding a white noise with a mean zero

https://doi.org/10.5194/hess-2021-181
Preprint. Discussion started: 18 May 2021

and standard deviation of 1 meter. The model parameters (i.e., channel roughness and bathymetry) are initialized using the Latin Hypercube Sampling method and evolved during the assimilation process. The ensemble of water depth values predicted by the model for the next time step together with observations, namely water stage and discharge at gauges are used in the multivariate Kalman equation to update the model parameters. The LISFLOOD-FP model is run for the second time with the updated parameters and the second multivariate Kalman equation uses the predicted water depth with observations to update the ensemble of water depth in the system. The ensemble of updated water depth (state), bathymetry, and channel roughness (parameters) ~~will be~~ used ~~with~~in the LISFLOOD-FP to predict an ensemble of water depth for the next time step. The predicted water depth is simply converted to a probabilistic flood inundation map. Using this data assimilation framework, we can generate 1-day forecast of probabilistic flood inundation maps which would be highly beneficial for real-time flood warning and decision making. It is worth mentioning that the forecasted probabilistic maps account for different sources of uncertainty including the forcing data (boundary condition flows), model parameters (channel roughness and bathymetry), and initial conditions (water depth).

The simulation period of the LISFLOOD-FP model is set up for 45 days from July-30-2017 to Sep-12-2017 and the entire month of July is used as a warm-up period. The water depth generated for the end of July ~~will be~~ used as the initial condition of the model. To account for the uncertainty of channel roughness and bathymetry, we sample ~~them~~ from uniform distributions ranging from [0,0.1] and [39,42] m, respectively. The bathymetry parameter is the elevation of ~~the~~ channel bed at the upper location of the channel. The offset parameter is calculated by subtracting this value from DEM at the upper location. Then, the bathymetry vector that includes the channel bed elevation for all channel cells is generated by subtracting the offset from DEM values along the

https://doi.org/10.5194/hess-2021-181
Preprint. Discussion started: 18 May 2021

Hydrology and Earth System Sciences
Open Access
Discussions

channel. It should be noted that the range of uniform distribution is chosen based on previous studies (Aronica et al., 2002b; Bales and Wagner, 2009; Di Baldassarre et al., 2009; Horritt, 2006; Pappenberger et al., 2008), expert judgment, and trial-and-error.

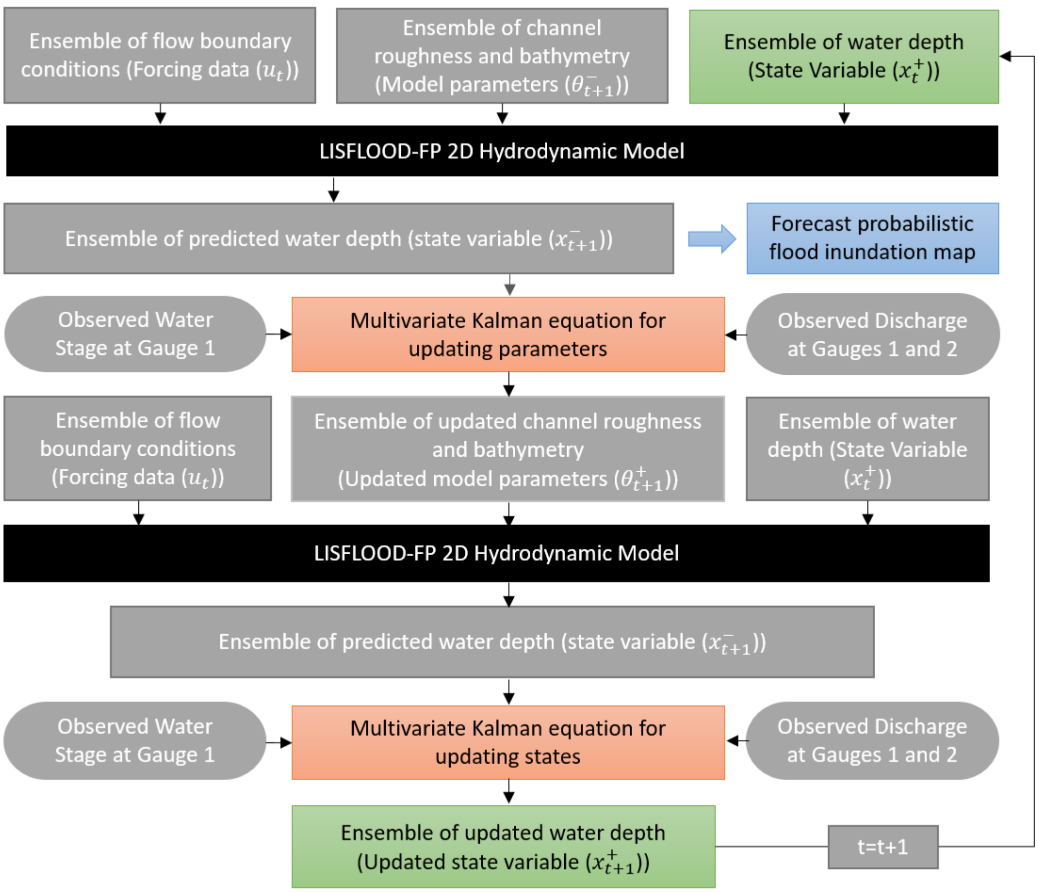

Figure 2. Schematic of the DA-hydrodynamic modeling framework for real-time probabilistic flood inundation mapping. The green boxes represent the state variables where their updated values are fed into the LISFLOOD-FP model and provide a probabilistic flood inundation map at the forecast mode (blue box). The black boxes highlight the physical model and the orange boxes represent the Kalman equations used for updating the parameter and state variables by the EnKF.

To assess the effectiveness and robustness of the proposed assimilation framework for probabilistic flood inundation mapping, we design three ~~different~~ experiments. First, an open-loop

(OL) simulation is established where the model is run without assimilation. In the second experiment, we perform DA-hydrodynamic modeling on a synthetic case study where we assume the model is perfect and has no error. In this approach, we set the model parameters (channel roughness and bathymetry), initial state (water depth) and boundary condition flows to fixed values and run the model to generate discharge and water surface elevation across the gauges within the study area. These predicted values are assumed as benchmark observations. This synthetic analysis ensures that the assimilation process performs well and the model parameters end up converging to predefined values. In the next step, we implement the proposed assimilation framework on a real case study where the observed discharge and ~~water surface elevation~~ data that are recorded from the USGS gauges during Hurricane Harvey, are assimilated into the model. Considering the severe flood condition during the Hurricane, we aim to investigate the extent to which the multivariate DA-Hydrodynamic modeling framework improves the model simulation and flood inundation mapping skill.

3.4 Validation strategy

As mentioned before, the convergence of uncertain model parameters toward truth in the synthetic experiment demonstrates the performance of DA-hydrodynamic modeling framework. To provide a robust analysis of each assimilation run, it is necessary to assess the model performance through multiple deterministic (KGE and RMSE) and probabilistic (NRR and Reliability) measures. The summary of performance measures used in this study is tabulated in Table 1.

https://doi.org/10.5194/hess-2021-181
Preprint. Discussion started: 18 May 2021

Table 1: Summary of performance measures used in this study

Performance Measure	Mathematical Representation
Kling-Gupta Efficiency (KGE)	$1-\sqrt{\left(\left(\frac{\mathrm{Cov}_{y_t y'_t}}{\sigma\sigma'}\right)-1\right)^2+\left(\left(\frac{\sigma'}{\sigma}\right)-1\right)^2+\left(\left(\frac{\mu'}{\mu}\right)-1\right)^2}$
Root Mean Square Error (RMSE)	$\sqrt{\frac{1}{T}\sum_{t=1}^{T}(y'_t-y_t)^2}$
Normalized Root-Mean-Square Error Ratio (NRR)	$\sqrt{\frac{1}{T}\sum_{t=1}^{T}\left(y_t-\overline{y'_{\blacksquare,t}}\right)^2}\times\left(\frac{1}{T}\left\{\sum_{t=1}^{T}\sqrt{\frac{1}{T}\left[\sum_{t=1}^{T}\left(y_t-\overline{y'_{\blacksquare,t}}\right)^2\right]}\right\}\sqrt{\frac{N+1}{2N}}\right)^{-1}$
Reliability	$1-\frac{2}{T}\sum_{t=1}^{T}\left\lvert\frac{Z_t}{T}-U_t\right\rvert$

y_t and y'_t are the observed and simulated values, respectively. The Kling–Gupta Efficiency (KGE) varies from $-\infty$ to 1, such that a value of 1 indicates a perfect fit between observed and simulated values. The pairs of (μ, σ) and (μ', σ') represent the first two statistical moments (means and standard deviations) of y_t and y'_t, respectively. Root mean squared error (RMSE) is the square root of the mean of the square of all of the error between the predicted and observed values.

NRR (DeChant and Moradkhani, 2012) is calculated to measure the ensemble spread and assess how confidently the ensemble mean is statistically distinguishable from the ensemble spread. Reliability (Renard et al., 2010) is a measure of the fit of the Q-Q quantile plot to a uniform. A value of 1 is exactly uniform and a value of 0 is the farthest possibility from uniform. For the description of the z_t and U_t calculation, we refer the readers to Renard et al. (2010).

The above four performance measures assess the dynamic behavior of DA-hydrodynamic modeling framework at two specific points. Moreover, to spatially evaluate the behavior of the proposed framework, we compare the maximum probabilistic flood inundation maps (union of probabilistic maps over the simulation period) with the observed floodplain map delineated aftermath of Harvey. The Receiver Operating Characteristic (ROC) graph is a common tool for validating probabilistic classifiers (Fawcett, 2006). Consider a deterministic flood map as a binary map where one and zero represent flooded and non-flooded cells, respectively. First, a threshold in the range of [0,1] is used to convert the probabilistic map to a binary deterministic map. This means all cells with the probability of inundation less than a given threshold are converted to zero and other cells are set to one. The binary map is compared with the reference map and the rate of true positive (rtp) and false positive (rfp) are calculated using Equations 7 and 8 (Jafarzadegan and Merwade, 2017):

$$rtp = \frac{True\ positive\ instances}{total\ positives} \quad (7)$$

$$rfp = \frac{False\ positive\ instances}{total\ negative} \quad (8)$$

where true and false positive instances represent the total number of flooded cells in the reference map that are predicted as flood and non-flooded cells, respectively. Total positives and negatives are total flooded and non-flooded cells in the reference map. This process is repeated and a set of points (rfp.rtp) are generated corresponding to different thresholds. The ROC graph connects the points in the rfp-rtp space and the area under the curve (AUC) represents the performance of the probabilistic classifier (Fawcett, 2006). In this study, we use AUC to compare the performance of OL simulation with the EnKF for probabilistic flood inundation mapping. In addition, we calculate

https://doi.org/10.5194/hess-2021-181
Preprint. Discussion started: 18 May 2021

the Underprediction and Overprediction Flood Indices (UFI and OFI) introduced by Jafarzadegan et al., (2018) for comparing probabilistic flood maps against deterministic reference maps:

$$UFI = \frac{\sum_{i=1}^{N}(1-P_i)}{N} \times 100 \qquad i \in F \tag{9}$$

$$OFI = \frac{\sum_{i=1}^{M}(P_j)}{M} \times 100 \qquad j \in NF \tag{10}$$

where F and NF denote the flooded and non-flooded regions in the reference map, and i and j are indicators of cells located within these regions. N and M are the total number of cells in the F and NF regions and P_i, P_j denote the probability of inundation for cells i and j derived from the probabilistic flood maps.

4. Results

4.1 Synthetic Case Study

We conduct the synthetic experiment to ensure the usefulness and effectiveness of the proposed DA-hydrodynamic modeling framework. Figure 3 presents uncertainty bound evolution of the parameters in the LISFLOOD-FP model (i.e., channel roughness and bathymetry) for 45 days assimilation of synthetic observations (i.e., discharge at gauges 1 and 2 and water stage at gauge 2). ~~The shaded areas correspond to 95, 75, 68, and 10 percentile predictive intervals, and the black stars at the end of each parameter subplot represent the true parameter values.~~ As seen both parameters converge smoothly to the certain region in parameter space where the uncertainty bounds stabilize. While the uncertainty bound associated with the bathymetry becomes stabilized at the early stage of the assimilation process, for the channel roughness, the uncertainty bound ~~gets~~ stabilized toward the end of the assimilation period. It is ~~also~~ evident from Figure 3 that the

https://doi.org/10.5194/hess-2021-181
Preprint. Discussion started: 18 May 2021

bathymetry is a more identifiable parameter as it shows the fastest convergence with a minimum degree of uncertainty. However, the channel roughness is less identifiable with the slowest convergence. ~~The scatter plots illustrate the evolution of parameter space at six different time segments.~~ The first day (t=1) includes all 100 ensemble members of parameters and day 30 corresponds to the highest discharge and water stage of flooding when the model parameters reach the highest improvement and ~~get~~ closer to the true value. Figure 3 shows that both model parameters are converging toward the true values as the assimilation proceeds. This indicates the efficacy and usefulness of the proposed DA-hydrodynamic modeling framework developed in this study.

https://doi.org/10.5194/hess-2021-181
Preprint. Discussion started: 18 May 2021

Hydrology and Earth System Sciences
Open Access
Discussions

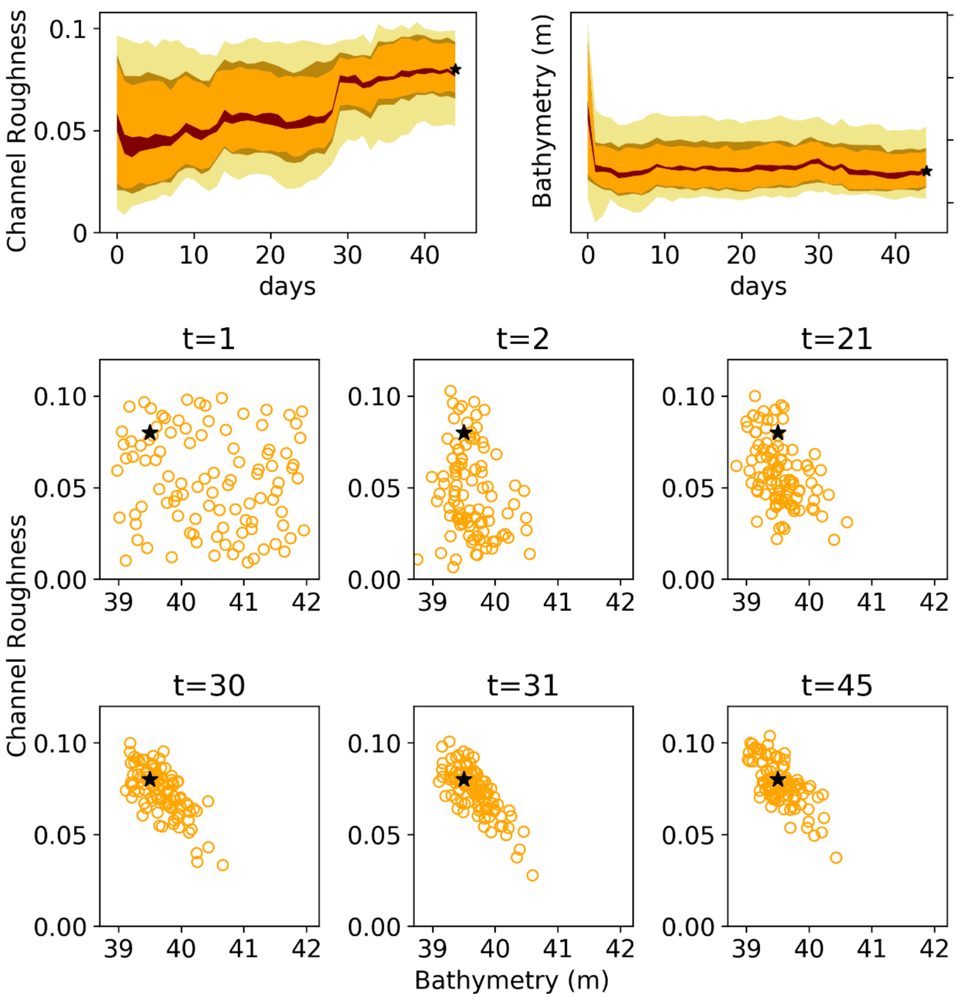

Figure 3. Temporal evolution of the LISFLOOD parameters for the synthetic experiment during Hurricane Harvey using the EnKF. (a) Temporal evolution of model parameter predictive intervals corresponding to 95, 75, 68, and 10 percentile (b) Temporal evolution of particle positions in the model parameter space at six different days during the Hurricane.

4.2 Real Case Study

In the real experiment, we assimilate the discharge and water stage readings from two ~~internal~~ USGS gauges into the LISFLOOD-FP model. We also run the OL simulation and calculate the ensemble mean to predict the discharge and water stage at these two gauges. Figure 4 presents a

https://doi.org/10.5194/hess-2021-181
Preprint. Discussion started: 18 May 2021

comparison of simulated discharge (Figures 4a~~,~~ 4b) and water stage (Figures 4c~~, ~~4d) with observations using both OL and our EnKF-based approach. Figures 4a and 4c are the prior estimates of discharge and water stage, while Figures 4b and 4d show their ~~posteriors~~ ~~which~~ reflect the updated variables after assimilating the observations into the model. It is worth mentioning that although ~~priors~~ represent the results before assimilating new observations into the model, their values are dependent on the initial conditions updated from observations in the previous time step. ~~In this study, ~~since forecasting (1-day lead time) is the main objective of DA-hydrodynamic modeling framework, we specifically focus on behavior of priors. As can be seen, the simulated peak discharge by the OL is highly overestimated by around 200 ~~cms~~ while assimilating the observations improve the results so that their difference with observation is less than 50 cms at the peak of the flood (KGE =0.76 and RMSE=40.9 ~~cms~~)). In contrast, the simulated water stage in Figures 4c and 4d are underestimated by OL by around 2 meters at the peak. Using the developed approach raises the peak of water stage at peak and reduces the errors significantly (KGE=0.96 and RMSE=0.5). The accurate estimates of prior discharge and water stage confirm the applicability of the proposed assimilation framework in forecast mode when real-time flood warning and decision making is the priority. The NRR measure for the prior discharge and water stage are 1.17 and 0.65 showing that the uncertainty bound is underestimated and overestimated, respectively. The reliability of both variables is above 70 percent since the uncertainty bounds encompass the observations for almost the entire simulation period.

https://doi.org/10.5194/hess-2021-181
Preprint. Discussion started: 18 May 2021

Hydrology and Earth System Sciences
Discussions

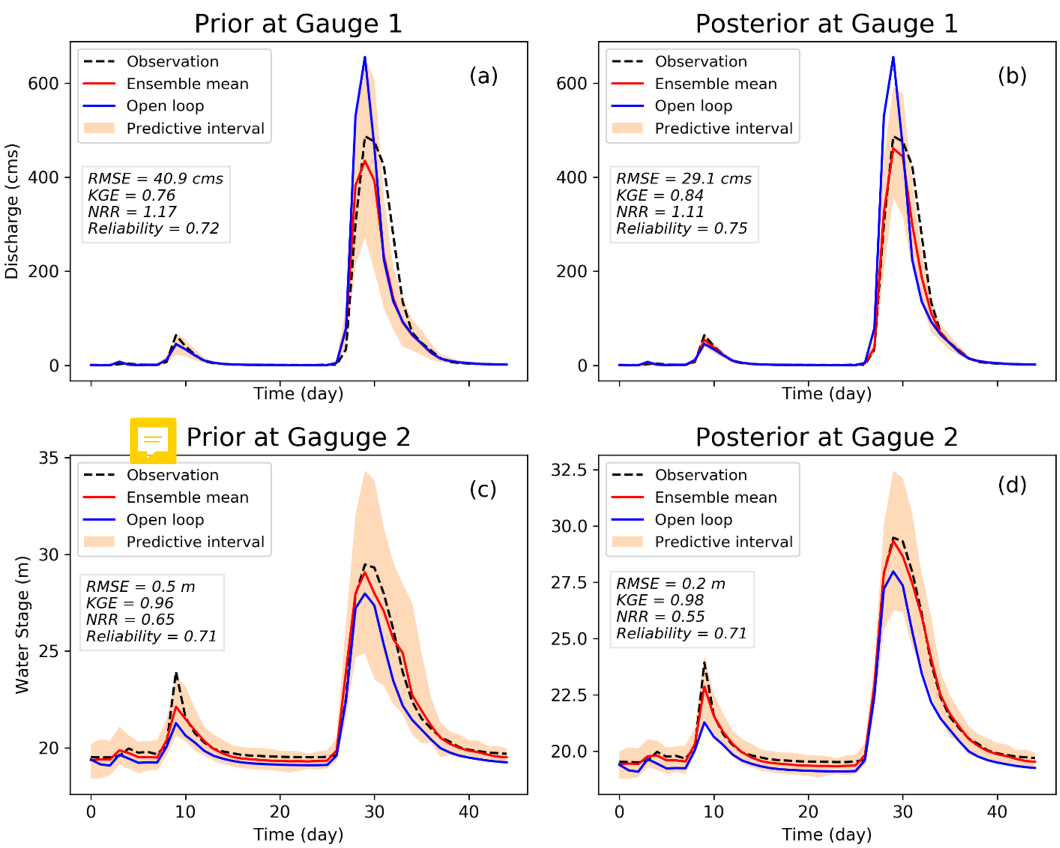

Figure 4 Simulation results of LISFLOOD-FP for the real experiment during Hurricane Harvey using the EnKF and open-loop. (a) Prior simulated discharge at gauge 1 (b) Posterior simulated discharge at gauge 1 (c) Prior simulated water stage at gauge 2 (d) Posterior simulated water stage at gauge 2. The shaded areas represent the predictive interval of simulated discharge and water stage by EnKF.

Figure 5 illustrates the prior and posterior distributions of discharge and water stage in the beginning, peak, and ending days of Hurricane Harvey flood. In all three days, the uncertainty bounds of both discharge and water stage are narrowed down by assimilating the observations so that posterior distributions are more precise compared to the priors. In the beginning and ending days (Aug 26 and Sep 1) the mean of prior distributions is substantially shifted toward truth in the posterior distributions. Figure 5 reveals that our developed approach provides more accurate and

https://doi.org/10.5194/hess-2021-181
Preprint. Discussion started: 18 May 2021

reliable posterior discharge and water stage distributions compared to prior distributions where the simulations are either overestimated or underestimated. It is noted that, on August 28 (day of flood peak), although the prior distributions accurately represent the observation, they have wide uncertainty bound. After correcting/updating the model state variables and parameters, as posterior distributions show, the uncertainty bound is reduced while the ensemble mean remains closer to the observation.

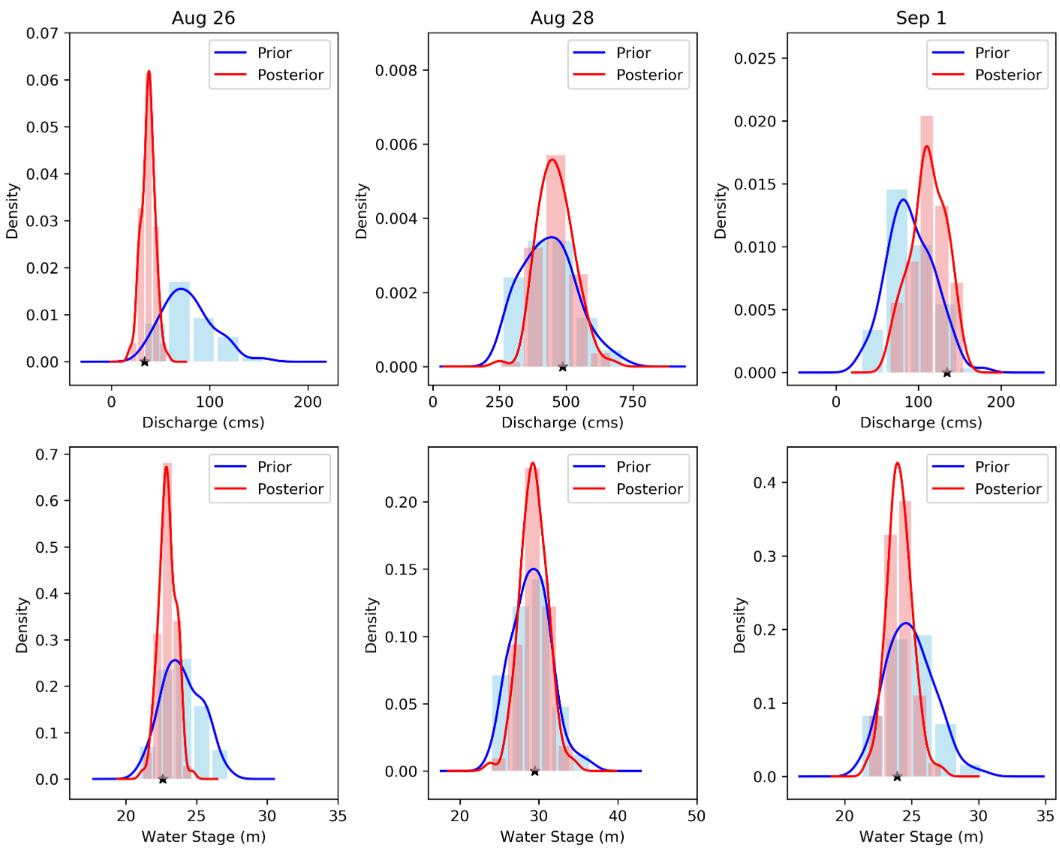

Figure 5. Prior and posterior distribution of discharge (a,b,c) and water stage (c,d,f) at the beginning (Aug 26), peak (Aug 28), and ending (Sep1) days of Hurricane Harvey using the EnKF

https://doi.org/10.5194/hess-2021-181
Preprint. Discussion started: 18 May 2021

Hydrology and Earth System Sciences
Discussions

4.3 Probabilistic Flood Inundation Mapping

In this ~~study~~, we ~~propose a DA-hydrodynamic modeling framework to~~ account for the uncertainties involved in flood modeling and generate real-time probabilistic flood inundation maps. Since the majority of flooding conditions occurred within ~~6~~ days from August 27-Sep 1, we display the spatial distribution of water depth in this period and provide probabilistic flood inundation maps using both OL and our developed approach (~~see~~ Figures 6 and 7). Figure 6 represents the first three days of Harvey, which corresponds to the upper limb of the flood hydrograph. On August 27, the major difference between the OL and EnKF appears in the regions around the upstream of the lower channel where the EnKF provides a more reliable inundated area. Moving toward the peak of flood on Aug 29, the OL generates a large region of uncertain cells around the banks of the upper channel while both the extent and density of uncertain values in the probabilistic maps generated by the EnKF is smaller during the peak of Harvey.

https://doi.org/10.5194/hess-2021-181
Preprint. Discussion started: 18 May 2021

Hydrology and Earth System Sciences
Open Access
EGU
Discussions

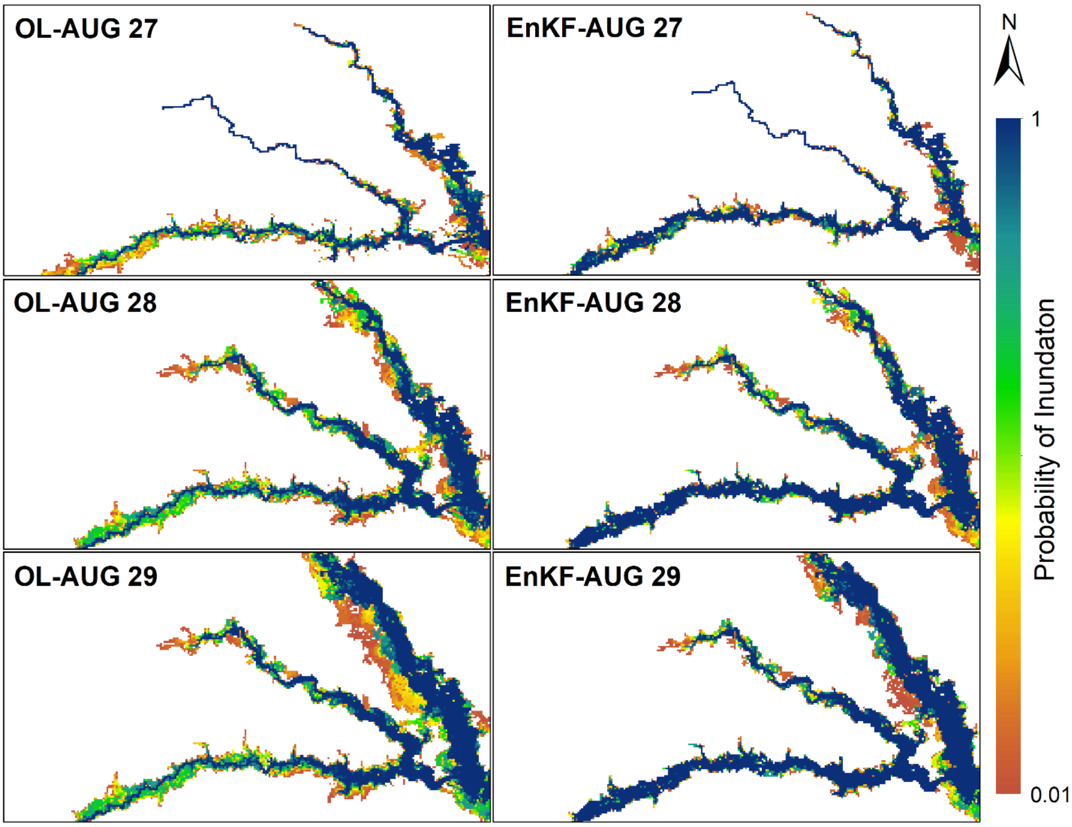

Figure 6 Probabilistic flood inundation maps generated by OL and EnKF techniques to simulate the upper limb of Harvey flood hydrograph from Aug 27 to Aug 29.

Figure 7 shows the probabilistic inundation areas in the last three days corresponding to the lower limb of the flood hydrograph. ~~In this figure,~~ the discrepancies between the OL and EnKF flood maps increase showing that performing DA is more effective in improving the inundation mapping skill from peak to ending point of the flood hydrograph. A large number of inundated cells generated by the OL are vanished after the peak of Harvey which results in a set of scattered discontinuous maps in Aug 31 and Sep 1. On the other hand, the probabilistic maps generated by the EnKF maintain their continuous shapes so that the probability of inundation is reduced without changing the extent. The merit of the EnKF in improving the flood inundation areas at the lower

https://doi.org/10.5194/hess-2021-181
Preprint. Discussion started: 18 May 2021

limb of the flood hydrograph agrees with results in Figures 4c and 4d where the EnKF widens the simulated water stage hydrographs and removes the lag difference that exists between the open-loop and observations.

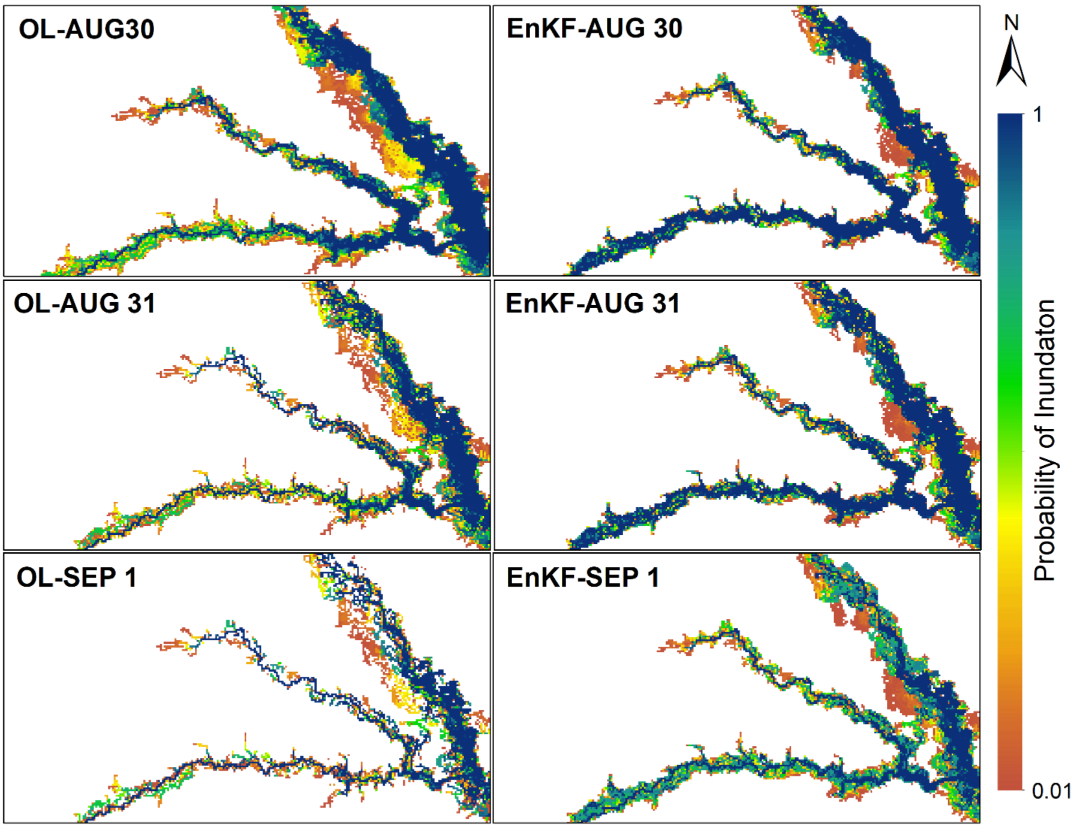

Figure 7 Probabilistic flood inundation maps generated by OL and EnKF techniques to simulate the lower limb of Harvey flood hydrograph from Aug 30 to Sep 1.

Finally, to quantify the performance of EnKF and OL for generating a spatial distribution of water depth over the domain, we illustrate the ROC graphs, the AUC values, and Fit indices in Figure 8. To calculate these measures, we ignore the temporal distributions and only report the maximum inundation maps that represent the union of flooded areas over the entire period of Harvey. Comparing the EnKF and OL in Figure 8.a, the EnKF line (blue) is closer to the northwest of the

https://doi.org/10.5194/hess-2021-181
Preprint. Discussion started: 18 May 2021

rfp-rtp space where its AUC is 5% higher than the OL approach. In Figure 8.b, each point represents the ~~Fit~~ indices for the OL and the EnKF approaches corresponding to a given threshold. Using ~~hundred number of~~ thresholds that ~~each ranging~~ from [0.01,1], the probabilistic maps are converted to 100 deterministic maps and the ~~Fit~~ indices are calculated. The position of scatters above the dash line confirms the EnKF outperforms the OL. In addition to these measures, the [UFI, OFI] indices calculated for OL and EnKF approaches are [30.3, 0.26] %~~,~~ and [23.4, 0.4]% respectively. The low values of OFI for both approaches (< 1%) show that the simulations mostly underestimate the flood inundation areas. In addition, comparing the indices of both approaches reveal that the EnKF reduces the overall underestimation by around 7%.

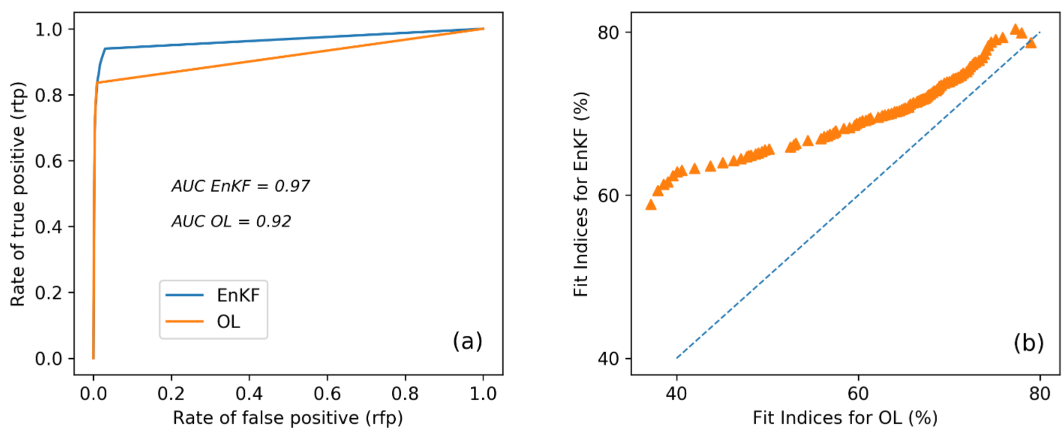

Figure 8 The Receiver Operating Curves (ROC) indicating the performance of OL and EnKF techniques for probabilistic flood inundation mapping

5. Discussion and Conclusions

The main motivation in this study is to propose a DA-hydrodynamic modeling framework for real-time probabilistic flood inundation mapping. Considering the coarse spatiotemporal resolution of satellite data for capturing the ~~water surface elevation~~, assimilating them into the hydrodynamic

https://doi.org/10.5194/hess-2021-181
Preprint. Discussion started: 18 May 2021

models may not be a practical solution for an upcoming flood event. On the other hand, the availability of daily discharge and ~~water surface elevation~~ data at gauge stations is a great opportunity to establish a multivariate DA-hydrodynamic modeling framework that updates the initial condition of modeling at daily scale and forecast the flood inundation areas at 1 day lead time. Here, we used the EnKF data assimilation method in conjunction with a hydrodynamic model to account for different sources of uncertainties involved in different layers of model simulations, including the boundary conditions, model parameters, and initial condition, and generate real-time probabilistic flood inundation maps. To further enhance the performance of the developed framework, the discharge and water stage at two different gauges are simultaneously assimilated into the LISFLOOD-FP model. The multivariate EnKF approach considers the correlation between discharge at two gauges and between discharge and ~~water surface elevation~~ at one gauge using a modified covariance matrix and Kalman gain equation.

In the synthetic experiment, we examined the convergence of model parameters toward truth and found that the proposed DA-hydrodynamic modeling framework can be successfully used to improve the accuracy and reliability of model predictions while accounting for uncertainties associated with model parameters. The channel roughness coefficient varied more rapidly than the bathymetry during the temporal evolutions of these parameters showing the better idemtifiability of this parameter. The validation results of the real experiment revealed that the assimilation with the EnKF approach improves the model predictions ~~at~~ across temporal and spatial scales (i.e., discharge and water stage time series at gauges and flood maps showing the maximum water depth over the simulation period). These improvements are more pronounced during the falling limb of the flood hydrograph where the EnKF widens the simulated hydrograph and removes the existing lag compared to the observations. Similarly, the simulated flood

https://doi.org/10.5194/hess-2021-181
Preprint. Discussion started: 18 May 2021

inundation maps confirm that the OL provides discontinuous scattered maps during the flood recession period while the EnKF provides a more accurate representation of the inundation areas. The validation results also demonstrate that the EnKF reduces the underestimation by 7% and outperformed the OL approach by around 5% for probabilistic flood inundation mapping.

To simulate flood hazards during the emergency of an upcoming flood event, using an efficient flood modeling framework is of paramount importance. However, a simplified model setup (i.e. using coarse resolution DEM, assuming uniform roughness coefficient for channel and floodplain, estimating bathymetry by lowering DEM with one parameter) for efficient flood modeling is prone to losing accuracy. Particularly, for an extreme flooding condition such as Hurricane Harvey, the simplified modeling may pose significant errors. The results obtained from the simulation of the real experiment demonstrated that despite using a simplified efficient modeling setup, we can still simulate the discharge, water stage, and inundation areas for an extreme flood event with acceptable accuracy while accounting for uncertainties involved in model predictions. This shows that assimilating the gauge data into a simplified model setup improves the accuracy, and provides an efficient probabilistic framework for real-time flood inundation mapping that considers potential sources of uncertainties in different layers of modeling.

The time dependency that exists between the upstream and downstream gauges along a channel can affect the performance of multivariate assimilation with those gauges. For future studies, using a more advanced DA technique that fully characterizes the model structural uncertainty (Abbaszadeh et al., 2019), and considering the time lag dependency between multiple gauges can improve the performance of modeling and provide more realistic assimilation of the hydrodynamic models. Finally, proposing a DA-hydrodynamic modeling framework that considers the DEM and

https://doi.org/10.5194/hess-2021-181
Preprint. Discussion started: 18 May 2021

Hydrology and Earth System Sciences
Discussions

channel width uncertainty can provide a more comprehensive uncertainty quantification for probabilistic flood inundation mapping in future studies.

Data availability

All the data used in this study, including the gauge streamflow and water stage data and the DEMs, are publicly available from the USGS website and National Elevation Dataset (NED). The reference flood maps provided for Hurricane Harvey is available from the USGS report at https://pubs.usgs.gov/sir/2018/5070/sir20185070.pdf.

Author contribution

KJ and PA designed the synthetic and real experiments. KJ developed, set up, evaluated and implemented the DA-hydrodynamic modeling framework for both experiments. PA provided inputs on the assimilation part. KJ wrote the first draft of the manuscript.HR and PA edited the manuscript.

Competing interests

The authors declare that they have no conflict of interest.

~~Acknowledgment~~

Partial financial support for this study was provided by the USACE contract #W912HZ2020055. We would like to thank the anonymous reviewers for their constructuve comments on the original version of the manuscript.

https://doi.org/10.5194/hess-2021-181
Preprint. Discussion started: 18 May 2021

References

Abbaszadeh, P., Gavahi, K., Moradkhani, H., 2020. Multivariate remotely sensed and in-situ data assimilation for enhancing community WRF-Hydro model forecasting. Adv. Water Resour. 145, 103721.

Abbaszadeh, P., Moradkhani, H., Daescu, D.N., 2019. The Quest for Model Uncertainty Quantification: A Hybrid Ensemble and Variational Data Assimilation Framework. Water Resour. Res. 55, 2407–2431. https://doi.org/10.1029/2018WR023629

Abbaszadeh, P., Moradkhani, H., Yan, H., 2018. Enhancing hydrologic data assimilation by evolutionary Particle Filter and Markov Chain Monte Carlo. Adv. Water Resour. 111, 192–204. https://doi.org/10.1016/j.advwatres.2017.11.011

Alemohammad, S.H., McLaughlin, D.B., Entekhabi, D., 2015. Quantifying precipitation uncertainty for land data assimilation applications. Mon. Weather Rev. 143, 3276–3299.

Anderson, J.L., Anderson, S.L., 1999. A Monte Carlo implementation of the nonlinear filtering problem to produce ensemble assimilations and forecasts. Mon. Weather Rev. 127, 2741–2758.

Aronica, G., Bates, P.D., Horritt, M.S., 2002a. Assessing the uncertainty in distributed model predictions using observed binary pattern information within GLUE. Hydrol. Process. 16, 2001–2016. https://doi.org/10.1002/hyp.398

Aronica, G., Bates, P.D., Horritt, M.S., 2002b. Assessing the uncertainty in distributed model predictions using observed binary pattern information within GLUE. Hydrol. Process. 16, 2001–2016. https://doi.org/10.1002/hyp.398

Azimi, S., Dariane, A.B., Modanesi, S., Bauer-Marschallinger, B., Bindlish, R., Wagner, W., Massari, C., 2020. Assimilation of Sentinel 1 and SMAP–based satellite soil moisture retrievals into SWAT hydrological model: The impact of satellite revisit time and product spatial resolution on flood simulations in small basins. J. Hydrol. 581, 124367.

Baldassarre, G.D., Schumann, G., Bates, P., 2009. Near real time satellite imagery to support and verify timely flood modelling. Hydrol. Process. 23, 799–803. https://doi.org/10.1002/hyp.7229

Bales, J.D., Wagner, C.R., 2009. Sources of uncertainty in flood inundation maps. J. Flood Risk Manag. 2, 139–147. https://doi.org/10.1111/j.1753-318X.2009.01029.x

Bates, P.D., De Roo, A.P.J., 2000. A simple raster-based model for flood inundation simulation. J. Hydrol. 236, 54–77. https://doi.org/10.1016/S0022-1694(00)00278-X

Brêda, J.P.L.F., Paiva, R.C.D., Bravo, J.M., Passaia, O.A., Moreira, D.M., 2019. Assimilation of Satellite Altimetry Data for Effective River Bathymetry. Water Resour. Res. 55, 7441–7463. https://doi.org/10.1029/2018WR024010

Clark, M.P., Hay, L.E., 2004. Use of Medium-Range Numerical Weather Prediction Model Output to Produce Forecasts of Streamflow. J. Hydrometeorol. 5, 15–32. https://doi.org/10.1175/1525-7541(2004)005<0015:UOMNWP>2.0.CO;2

Courtier, P., Derber, J., Errico, R.O.N., Louis, J.-F., VukiĆEviĆ, T., 1993. Important literature on the use of adjoint, variational methods and the Kalman filter in meteorology. Tellus Dyn. Meteorol. Oceanogr. 45, 342–357.

Cuo, L., Pagano, T.C., Wang, Q.J., 2011. A Review of Quantitative Precipitation Forecasts and Their Use in Short- to Medium-Range Streamflow Forecasting. J. Hydrometeorol. 12, 713–728. https://doi.org/10.1175/2011JHM1347.1

DeChant, C.M., Moradkhani, H., 2014. Toward a reliable prediction of seasonal forecast uncertainty: Addressing model and initial condition uncertainty with ensemble data assimilation and sequential Bayesian combination. J. Hydrol. 519, 2967–2977.

Di Baldassarre, G., Schumann, G., Bates, P.D., 2009. A technique for the calibration of hydraulic models using uncertain satellite observations of flood extent. J. Hydrol. 367, 276–282. https://doi.org/10.1016/j.jhydrol.2009.01.020

Domeneghetti, A., Vorogushyn, S., Castellarin, A., Merz, B., Brath, A., 2013. Probabilistic flood hazard mapping: effects of uncertain boundary conditions. Hydrol. Earth Syst. Sci. 17, 3127–3140.

Durand, M., Andreadis, K.M., Alsdorf, D.E., Lettenmaier, D.P., Moller, D., Wilson, M., 2008. Estimation of bathymetric depth and slope from data assimilation of swath altimetry into a hydrodynamic model. Geophys. Res. Lett. 35.

Fawcett, T., 2006. An introduction to ROC analysis. Pattern Recognit. Lett., ROC Analysis in Pattern Recognition 27, 861–874. https://doi.org/10.1016/j.patrec.2005.10.010

García-Pintado, J., Neal, J.C., Mason, D.C., Dance, S.L., Bates, P.D., 2013. Scheduling satellite-based SAR acquisition for sequential assimilation of water level observations into flood modelling. J. Hydrol. 495, 252–266. https://doi.org/10.1016/j.jhydrol.2013.03.050

Giustarini, L., Matgen, P., Hostache, R., Montanari, M., Plaza Guingla, D.A., Pauwels, V., De Lannoy, G., De Keyser, R., Pfister, L., Hoffmann, L., 2011. Assimilating SAR-derived water level data into a hydraulic model: a case study. Hydrol. Earth Syst. Sci. 15, 2349–2365.

Gobeyn, S., Van Wesemael, A., Neal, J., Lievens, H., Eerdenbrugh, K.V., De Vleeschouwer, N., Vernieuwe, H., Schumann, G.J.-P., Di Baldassarre, G., Baets, B.D., Bates, P.D., Verhoest, N.E.C., 2017. Impact of the timing of a SAR image acquisition on the calibration of a flood inundation model. Adv. Water Resour. 100, 126–138. https://doi.org/10.1016/j.advwatres.2016.12.005

Habets, F., LeMoigne, P., Noilhan, J., 2004. On the utility of operational precipitation forecasts to served as input for streamflow forecasting. J. Hydrol. 293, 270–288. https://doi.org/10.1016/j.jhydrol.2004.02.004

Hall, J.W., Tarantola, S., Bates, P.D., Horritt, M.S., 2005. Distributed Sensitivity Analysis of Flood Inundation Model Calibration. J. Hydraul. Eng. 131, 117–126. https://doi.org/10.1061/(ASCE)0733-9429(2005)131:2(117)

Horritt, M.S., 2006. A methodology for the validation of uncertain flood inundation models. J. Hydrol. 326, 153–165. https://doi.org/10.1016/j.jhydrol.2005.10.027

https://doi.org/10.5194/hess-2021-181
Preprint. Discussion started: 18 May 2021

Hostache, R., Chini, M., Giustarini, L., Neal, J., Kavetski, D., Wood, M., Corato, G., Pelich, R.-M., Matgen, P., 2018. Near-Real-Time Assimilation of SAR-Derived Flood Maps for Improving Flood Forecasts. Water Resour. Res. 54, 5516–5535. https://doi.org/10.1029/2017WR022205

Hostache, R., Lai, X., Monnier, J., Puech, C., 2010. Assimilation of spatially distributed water levels into a shallow-water flood model. Part II: Use of a remote sensing image of Mosel River. J. Hydrol. 390, 257–268. https://doi.org/10.1016/j.jhydrol.2010.07.003

Hostache, R., Matgen, P., Schumann, G., Puech, C., Hoffmann, L., Pfister, L., 2009. Water Level Estimation and Reduction of Hydraulic Model Calibration Uncertainties Using Satellite SAR Images of Floods. IEEE Trans. Geosci. Remote Sens. 47, 431–441. https://doi.org/10.1109/TGRS.2008.2008718

Hunter, N.M., Bates, P.D., Horritt, M.S., De Roo, A.P.J., Werner, M.G.F., 2005. Utility of different data types for calibrating flood inundation models within a GLUE framework. Hydrol. Earth Syst. Sci. Discuss. 9, 412–430.

Jafarzadegan, K., Merwade, V., 2017. A DEM-based approach for large-scale floodplain mapping in ungauged watersheds. J. Hydrol. 550, 650–662. https://doi.org/10.1016/j.jhydrol.2017.04.053

Jafarzadegan, K., Merwade, V., Saksena, S., 2018. A geomorphic approach to 100-year floodplain mapping for the Conterminous United States. J. Hydrol. 561, 43–58. https://doi.org/10.1016/j.jhydrol.2018.03.061

Kumar, S.V., Dong, J., Peters-Lidard, C.D., Mocko, D., Gómez, B., 2017. Role of forcing uncertainty and background model error characterization in snow data assimilation. Hydrol. Earth Syst. Sci. 21, 2637–2647.

Lai, X., Liang, Q., Yesou, H., Daillet, S., 2014. Variational assimilation of remotely sensed flood extents using a 2-D flood model. Hydrol. Earth Syst. Sci. 18.

Leach, J.M., Kornelsen, K.C., Coulibaly, P., 2018. Assimilation of near-real time data products into models of an urban basin. J. Hydrol. 563, 51–64.

Lee, H., Seo, D.-J., Koren, V., 2011. Assimilation of streamflow and in situ soil moisture data into operational distributed hydrologic models: Effects of uncertainties in the data and initial model soil moisture states. Adv. Water Resour. 34, 1597–1615.

Lievens, H., Reichle, R.H., Liu, Q., De Lannoy, G.J., Dunbar, R.S., Kim, S.B., Das, N.N., Cosh, M., Walker, J.P., Wagner, W., 2017. Joint Sentinel-1 and SMAP data assimilation to improve soil moisture estimates. Geophys. Res. Lett. 44, 6145–6153.

Maidment, D.R., 2017. Conceptual Framework for the National Flood Interoperability Experiment. JAWRA J. Am. Water Resour. Assoc. 53, 245–257. https://doi.org/10.1111/1752-1688.12474

Mason, D.C., Bates, P.D., Dall'Amico, J.T., 2009. Calibration of uncertain flood inundation models using remotely sensed water levels. J. Hydrol. 368, 224–236.

Matgen, P., Montanari, M., Hostache, R., Pfister, L., Hoffmann, L., Plaza, D., Pauwels, V.R.N., De Lannoy, G., De Keyser, R., Savenije, H.H.G., 2010a. Towards the sequential

https://doi.org/10.5194/hess-2021-181
Preprint. Discussion started: 18 May 2021

Hydrology and Earth System Sciences
Discussions

assimilation of SAR-derived water stages into hydraulic models using the Particle Filter: proof of concept. Hydrol. Earth Syst. Sci. 14, 1773–1785.

Matgen, P., Montanari, M., Hostache, R., Pfister, L., Hoffmann, L., Plaza, D., Pauwels, V.R.N., De Lannoy, G., De Keyser, R., Savenije, H.H.G., 2010b. Towards the sequential assimilation of SAR-derived water stages into hydraulic models using the Particle Filter: proof of concept. Hydrol. Earth Syst. Sci. 14, 1773–1785.

Merwade, V., Cook, A., Coonrod, J., 2008. GIS techniques for creating river terrain models for hydrodynamic modeling and flood inundation mapping. Environ. Model. Softw. 23, 1300–1311. https://doi.org/10.1016/j.envsoft.2008.03.005

Moradkhani, H., Hsu, K.-L., Gupta, H., Sorooshian, S., 2005a. Uncertainty assessment of hydrologic model states and parameters: Sequential data assimilation using the particle filter. Water Resour. Res. 41.

Moradkhani, H., Nearing, G.S., Abbaszadeh, P., Pathiraja, S., 2019. Fundamentals of data assimilation and theoretical advances. Handb. Hydrometeorol. Ensemble Forecast. Springer Berl. Heidelb. Berl. Heidelb. 675–699.

Moradkhani, H., Sorooshian, S., Gupta, H.V., Houser, P.R., 2005b. Dual state–parameter estimation of hydrological models using ensemble Kalman filter. Adv. Water Resour. 28, 135–147. https://doi.org/10.1016/j.advwatres.2004.09.002

Munier, S., Polebistki, A., Brown, C., Belaud, G., Lettenmaier, D.P., 2015. SWOT data assimilation for operational reservoir management on the upper Niger River Basin. Water Resour. Res. 51, 554–575. https://doi.org/10.1002/2014WR016157

Neal, J., Keef, C., Bates, P., Beven, K., Leedal, D., 2013. Probabilistic flood risk mapping including spatial dependence. Hydrol. Process. 27, 1349–1363. https://doi.org/10.1002/hyp.9572

Neal, J., Schumann, G., Bates, P., 2012. A subgrid channel model for simulating river hydraulics and floodplain inundation over large and data sparse areas. Water Resour. Res. 48. https://doi.org/10.1029/2012WR012514

Neal, J., Schumann, G., Bates, P., Buytaert, W., Matgen, P., Pappenberger, F., 2009. A data assimilation approach to discharge estimation from space. Hydrol. Process. 23, 3641–3649. https://doi.org/10.1002/hyp.7518

Pappenberger, F., Beven, K.J., Ratto, M., Matgen, P., 2008. Multi-method global sensitivity analysis of flood inundation models. Adv. Water Resour. 31, 1–14. https://doi.org/10.1016/j.advwatres.2007.04.009

Pappenberger, F., Frodsham, K., Beven, K., Romanowicz, R., Matgen, P., 2007. Fuzzy set approach to calibrating distributed flood inundation models using remote sensing observations. Hydrol. Earth Syst. Sci. Discuss. 11, 739–752.

Pathiraja, S., Moradkhani, H., Marshall, L., Sharma, A., Geenens, G., 2018. Data-driven model uncertainty estimation in hydrologic data assimilation. Water Resour. Res. 54, 1252–1280.

Pauwels, V.R., Hoeben, R., Verhoest, N.E., De Troch, F.P., 2001. The importance of the spatial patterns of remotely sensed soil moisture in the improvement of discharge predictions for small-scale basins through data assimilation. J. Hydrol. 251, 88–102.
Pedinotti, V., Boone, A., Ricci, S., Biancamaria, S., Mognard, N., 2014. Assimilation of satellite data to optimize large-scale hydrological model parameters: a case study for the SWOT mission. Hydrol. Earth Syst. Sci. 18, 4485–4507. https://doi.org/10.5194/hess-18-4485-2014
Pedrozo-Acuña, A., Rodríguez-Rincón, J.P., Arganis-Juárez, M., Domínguez-Mora, R., Villareal, F.J.G., 2015. Estimation of probabilistic flood inundation maps for an extreme event: Pánuco River, México. J. Flood Risk Manag. 8, 177–192. https://doi.org/10.1111/jfr3.12067
Pinter, N., Santos, N., Hui, R., 2017. Preliminary analysis of Hurricane Harvey flooding in Harris County, Texas. Retrieved UC Davis Cent. Watershed Sci.-Calif. WaterBlog Httpscaliforniawaterblog Com20170901preliminary-Anal.--Hurricaneharvey-Flooding--Harris-Cty.-Tex.
Purvis, M.J., Bates, P.D., Hayes, C.M., 2008. A probabilistic methodology to estimate future coastal flood risk due to sea level rise. Coast. Eng. 55, 1062–1073. https://doi.org/10.1016/j.coastaleng.2008.04.008
Rahman, Md.R., Thakur, P.K., 2018. Detecting, mapping and analysing of flood water propagation using synthetic aperture radar (SAR) satellite data and GIS: A case study from the Kendrapara District of Orissa State of India. Egypt. J. Remote Sens. Space Sci., EJRS Special Issue: Microwave Remote Sensing in honor of Professor Adel Yehia 21, S37–S41. https://doi.org/10.1016/j.ejrs.2017.10.002
Reichle, R.H., McLaughlin, D.B., Entekhabi, D., 2002. Hydrologic data assimilation with the ensemble Kalman filter. Mon. Weather Rev. 130, 103–114.
Renard, B., Kavetski, D., Kuczera, G., Thyer, M., Franks, S.W., 2010. Understanding predictive uncertainty in hydrologic modeling: The challenge of identifying input and structural errors. Water Resour. Res. 46. https://doi.org/10.1029/2009WR008328
Romanowicz, R., Beven, K., 2003. Estimation of flood inundation probabilities as conditioned on event inundation maps. Water Resour. Res. 39. https://doi.org/10.1029/2001WR001056
Sheffield, J., Pan, M., Wood, E.F., Mitchell, K.E., Houser, P.R., Schaake, J.C., Robock, A., Lohmann, D., Cosgrove, B., Duan, Q., Luo, L., Higgins, R.W., Pinker, R.T., Tarpley, J.D., Ramsay, B.H., 2003. Snow process modeling in the North American Land Data Assimilation System (NLDAS): 1. Evaluation of model-simulated snow cover extent. J. Geophys. Res. Atmospheres 108. https://doi.org/10.1029/2002JD003274
Slater, A.G., Clark, M.P., 2006. Snow data assimilation via an ensemble Kalman filter. J. Hydrometeorol. 7, 478–493.

https://doi.org/10.5194/hess-2021-181
Preprint. Discussion started: 18 May 2021

Tarpanelli, A., Brocca, L., Melone, F., Moramarco, T., 2013. Hydraulic modelling calibration in small rivers by using coarse resolution synthetic aperture radar imagery. Hydrol. Process. 27, 1321–1330. https://doi.org/10.1002/hyp.9550

Teng, J., Jakeman, A.J., Vaze, J., Croke, B.F.W., Dutta, D., Kim, S., 2017. Flood inundation modelling: A review of methods, recent advances and uncertainty analysis. Environ. Model. Softw. 90, 201–216. https://doi.org/10.1016/j.envsoft.2017.01.006

Vrugt, J.A., Gupta, H.V., Nualláin, B., Bouten, W., 2006. Real-time data assimilation for operational ensemble streamflow forecasting. J. Hydrometeorol. 7, 548–565.

Yoon, Y., Durand, M., Merry, C.J., Clark, E.A., Andreadis, K.M., Alsdorf, D.E., 2012a. Estimating river bathymetry from data assimilation of synthetic SWOT measurements. J. Hydrol. 464, 363–375.

Yoon, Y., Durand, M., Merry, C.J., Clark, E.A., Andreadis, K.M., Alsdorf, D.E., 2012b. Estimating river bathymetry from data assimilation of synthetic SWOT measurements. J. Hydrol. 464, 363–375.

Zhang, Q., Shi, L., Holzman, M., Ye, M., Wang, Y., Carmona, F., Zha, Y., 2019. A dynamic data-driven method for dealing with model structural error in soil moisture data assimilation. Adv. Water Resour. 132, 103407.